PCCP

Accepted Manuscript

ROYAL SOCIETY OF CHEMISTRY

www.rsc.org/pccp

Cite this: DOI: 10.1039/c0xx00000x

www.rsc.org/xxxxxx

ARTICLE TYPE

Use of UV/ozone-treated MoS_2 nanosheets for extended air stability in organic photovoltaic cells

Quyet Van Le[a], Thang Phan Nguyen[a], Ho Won Jang[b], and Soo Young Kim[a,*]

Received (in XXX, XXX) Xth XXXXXXXXX 20XX, Accepted Xth XXXXXXXXX 20XX

DOI: 10.1039/b000000x

MoS_2 nanosheets obtained through a simple sonication exfoliation method are employed as a hole-extraction layer (HEL) to improve the efficiency and air stability of organic photovoltaic cells (OPVs). The reduction in the wavenumber difference, appearance of a UV-vis peak, and atomic force microscopy images indicate that MoS_2 nanosheets are formed through the sonication method. The OPVs with MoS_2 layers show a degraded performance with a power conversion efficiency (PCE) of 1.08%, which is lower than that of OPVs without HEL (1.84%). After performing the UV/ozone (UVO) treatment of the MoS_2 surface for 15 min, the PCE value increases to 2.44%. Synchrotron radiation photoelectron spectroscopy data show that the work function of MoS2 increases from 4.6 to 4.9 eV upon UVO treatment, suggesting that the increase in the PCE value is caused by the bandgap alignment. Upon inserting poly(3,4-ethylenedioxythiophene):poly(styrene sulfonate) (PEDOT:PSS) between MoS_2 and the active layer, the PCE value of the OPV increases to 2.81%, which is comparable with that of the device employing only PEDOT:PSS. Furthermore, the stability of the OPVs is improved significantly when MoS_2/PEDOT:PSS layers are used as the HEL. Therefore, it is considered that the use of UVO-treated MoS_2 may improve the stability of OPV cells without degrading the device performance.

1 Introduction

Recently, organic photovoltaic cells (OPVs) have attracted much attention because of their low cost, light weight, flexibility, and ease of enlargement through the roll-to-roll coating process.[1-3] The most common materials for OPV fabrication are poly(3-hexylthiophene) (P3HT) as the donor and [6,6]-phenyl-C61-butyric acid methyl ester (PCBM) as the acceptor, which are used because of their good solubilities in common solvents. One strategy for improving the performance of OPVs is to insert a buffer layer between the active layer and the electrode to facilitate the collection of holes and electrons. Other approaches for improving the light harvesting of OPVs include the synthesis of new polymers or the tuning of the absorption of the active layer to a suitable wavelength range.[4-7] Poly(3,4-ethylenedioxythiophene):poly(styrene-sulfonate) (PEDOT:PSS) is widely used as a hole-extraction layer (HEL). However, it has been reported that PEDOT:PSS is not suitable for practical applications owing to its hygroscopicity and acidity, which causes fast degradation of OPVs.[8-10] To resolve this problem, transition-metal oxides such as molybdenum oxide (MoO_3),[11-13] vanadium oxide (Va_2O_5),[13, 14] nickel oxide (NiO),[15] and tungsten oxide (WO_3),[16, 17] are under intensive investigation as possible substitutes for PEDOT:PSS. Ultrathin two-dimensional nanosheets of transition-metal sulfides have also attracted much interest because of their superior mechanical and electrical properties such as their thermal conductivity and carrier mobility.[18-20] The application of MoS_x as the HEL in OPVs has also been reported recently.[21-24] However, the use of transition-metal sulfides in OPVs remains a great challenge because of the difficulties inherent in the exfoliation process for the synthesis of MoS_2 and a mismatch of the work function between the MoS_2 HEL and the active layer. Therefore, in this study, a simple sonication process is used to make MoS_2 nanosheets, and the UV/ozone (UVO) treatment method is utilized for modulating the work function of the MoS_2 layer to improve the performance and stability of the OPVs.

In this work, UVO-treated MoS_2 was used as the HEL in OPVs to extend their stability. Ultrathin nanosheets of MoS_2 obtained through the sonication method were spin-coated on indium tin oxide (ITO)/glass substrates to afford a uniform and complete single layer. Raman spectroscopy was performed to identify the effect of the thickness after the sonication process. UV-vis absorption spectroscopy was used to investigate the change in the bandgap, while the thickness and size of the MoS_2 nanosheets were confirmed by atomic force microscopy (AFM). Synchrotron radiation photoemission spectroscopy (SRPES) was used to investigate the effect of the UVO treatment on the atomic composition and work function of MoS_2. On the basis of these measurements, the effect of UVO-treated MoS_2 as the HEL in OPVs is discussed.

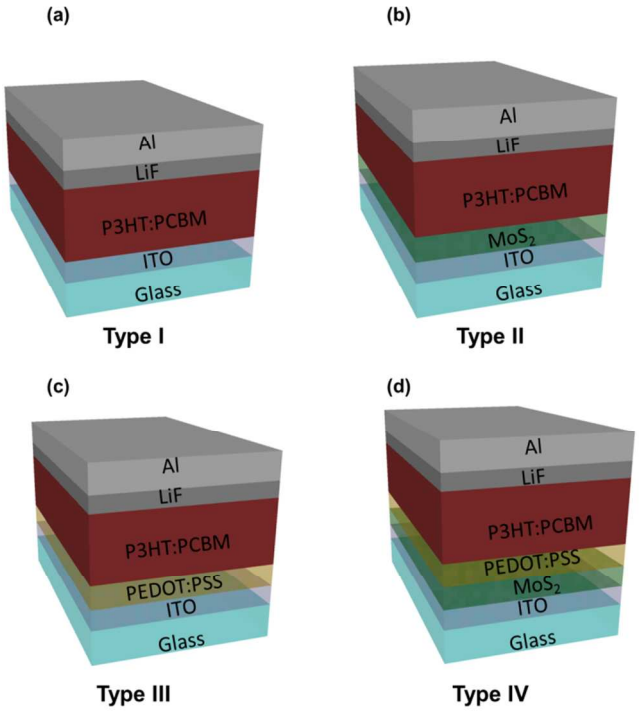

Fig. 1 Structures of OPVs fabricated in this experiment. (a) (Type I) ITO/P3HT:PCBM/LiF/Al, (b) (Type II) ITO/MoS_2/P3HT:PCBM/LiF/Al, (c) (Type III) ITO/PEDOT:PSS/P3HT:PCBM/LiF/Al, and (d) (Type IV) ITO/MoS_2/PEDOT:PSS/P3HT:PCBM/LiF/Al.

2 Experimental section

MoS_2 powder and N-vinyl-2-pyrrolidone (NVP) were purchased from Sigma–Aldrich. An ultrasonicator (Sonicator Microtip Probes, SONICS VCX-750) was used to induce the exfoliation of the MoS_2 powder. MoS_2 (200 mg) was mixed with NVP solvent (40 mL) in an 80-mL flask. The solution was sonicated with power of 200 W for 8 h, which was the optimized condition for this experiment. After sonication, the samples were centrifuged using a DAIHAN WiseSpin CF-10 instrument at 10,000 rpm for 10 min. The floating solution, which contained the exfoliated MoS_2 layer of small-diameter, was collected with a pipette. Then, the solvent was removed by washing with ethanol, and the final product was dried at 30 °C in a vacuum oven.

A patterned ITO glass substrate was utilized for OPV fabrication. First, the substrate was cleaned sequentially with acetone, isopropyl alcohol, and deionized water for 15 min each, with ultrasonic assistance. Then, the cleaned ITO glass was dried at 80 °C for 15 min before performing the UVO treatment for 15 min. Four types of OPVs were fabricated, as shown in Fig. 1: ITO/P3HT:PCBM/LiF/Al (Type I), ITO/MoS_2/P3HT:PCBM/LiF/Al (Type II), ITO/PEDOT:PSS/P3HT:PCBM/LiF/Al (Type III), and ITO/MoS_2/PEDOT:PSS/P3HT:PCBM/LiF/Al (Type IV). The ultrathin layer of MoS_2 was spin-coated at a rate of 5000 rpm for 30 s in dimethylformamide (DMF) solvent. PEDOT:PSS was spin-coated at a rate of 4000 rpm for 30 s. Subsequently, the films were annealed at 150 °C for 30 min under a N_2 atmosphere in a glove box. P3HT:PCBM in a 6:4 weight ratio with a concentration of 30 mg/mL in 1,2-dichlorobenzene was spin-coated at 700 rpm for 30 s and annealed at 110 °C for 10 min. Finally, the cathode with LiF (1-nm thickness) and Al (100-nm thickness) was thermally deposited at a base pressure of 2×10^{-6} Torr. The active area of the device was approximately 4 mm^2.

Raman spectra for investigating the changes in the thickness of the exfoliated MoS_2 were obtained with LabRAM HR (Horiba Jobin Yvon, Japan) at an excitation wavelength of 514.54 nm. UV-vis absorption spectra were collected with a V-670 UV-vis spectrophotometer. AFM (XE-100/PSIA) in the contact mode was employed to confirm the thickness of the exfoliated MoS_2. SPRES experiments were performed in an ultra-high-vacuum chamber (base pressure of $\approx 10^{-10}$ Torr) with a 4D beam line, equipped with an electron analyzer and a heating element, at the Pohang Acceleration Laboratory. The onset of photoemission, corresponding to the vacuum level at the surface of MoS_2, was measured using an incident photon energy of 250 eV with a negative bias on the sample. The results were corrected for charging effects by using Au 4f as an internal reference. The current density–voltage (J–V) curve was measured in air with a Keithley 2612 source meter under AM 1.5 G illumination (100 mW/cm^2). The maximum power conversion efficiency (PCE) for the conversion of solar radiation to electrical power was calculated using the equation

$$\frac{V_{oc} \times J_{sc} \times FF}{P_{in}(=100 mW/cm^{-2})} \times 100$$

, where V_{oc} is the open-circuit voltage, J_{sc} is the short-circuit current density, FF is the fill factor, and P_{in} is the illumination power.

3 Results and discussion

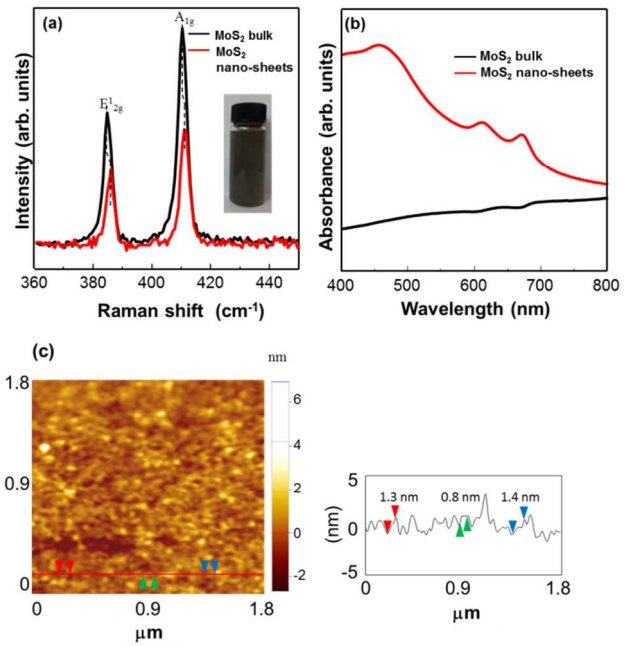

Fig. 2(a) Raman spectra of MoS_2 bulk and MoS_2 nanosheets, (b) UV-vis absorption spectra of MoS_2 bulk and MoS_2 nanosheets, and (c) AFM image of MoS_2 nanosheets spin-coated on the SiO_2/Si substrate. The height difference is shown along the red line in the AFM image.

Figure 2(a) shows the Raman spectra of bulk MoS_2 and MoS_2 nanosheets. Two optical phonon modes (E^1_{2g} and A^1_g) and one longitudinal acoustic mode are observed in ultrathin and bulk

MoS_2; E^1_{2g} is an in-plane optical mode, whereas A^1_g corresponds to out-of-plane vibrations of the sulfur atoms.[25] For bulk MoS_2, the E^1_{2g} and A^1_g modes appear at approximately 384 and 410 cm^{-1}, respectively. The frequencies of these modes are similar to the reported values from Raman and neutron scattering.[26] After sonication, the E^1_{2g} and A^1_g modes in the exfoliated MoS_2 nanosheets appear at 386 and 411 cm^{-1}, respectively. The increase in wavenumber for both peaks corresponds with the results of a previous report.[27] The energy difference between E^1_{2g} and A^1_g was reduced by the sonication process, suggesting a decrease in the layer thickness.[28] The UV-vis absorption spectra of bulk MoS_2 and MoS_2 nanosheets are shown in Fig. 2(b). No peak was detected in the bulk MoS_2 sample; it is believed that bulk MoS_2 has an indirect bandgap, and therefore, its absorption peak does not appear in the UV-vis absorption spectrum. After the sonication process, absorption peaks appeared at 460, 610, and 671 nm, indicating that the indirect bandgap had changed to a direct bandgap owing to the exfoliation process. These peaks correspond to 2.7, 2.03, and 1.85 eV, which are the same as the values reported for the bandgap energy of single-layer MoS_2.[29] Figure 2(c) shows an AFM image of MoS_2 nanosheets spin-coated on the SiO_2/Si substrate. Many small particles of MoS_2 are seen in the image. The height difference was measured along the red line in the AFM image. The thicknesses of individual particles, indicated by two triangles of the same color, were 1.3, 0.8, and 1.4 nm. This result confirmed that the thickness and lateral size of the MoS_2 nanosheets exfoliated through the sonication method were approximately 1 and 100–300 nm, respectively, in agreement with the results for MoS_2 nanosheets exfoliated by the lithium intercalation method.[17] These data indicate that bulk MoS_2 was changed to MoS_2 nanosheets upon sonication.

Figure 3 shows the (a) Mo 3d and (b) O 1s spectra of the MoS_2 films as a function of the UVO treatment time. The surface contaminations of the spin-coated MoS_2 sample were removed with argon ions before SRPES measurement. Two main peaks of Mo 3d are located at 228.5 and 231.63 eV in the spin-coated sample, which correspond to Mo^{4+} $d_{5/2}$ and Mo^{4+} $d_{3/2}$ of MoS_2.[24] After performing the UVO treatment for 15 and 30 min, two new peaks appeared, at 232.7 and 235.6 eV, which correspond to $Mo^{6+}{}_{5/2}$ and $Mo^{6+}{}_{3/2}$ of MoO_3.[24, 30] As the UVO treatment time was prolonged, the Mo^{4+} intensity decreased. The appearance of Mo^{6+} and decrease in the Mo^{4+} intensity indicated that MoS_2 was changed to MoO_x by UVO treatment. In the case of the O 1s spectra, the peak of O 1s was located at 532.3 eV in the spin-coated MoS_2 sample, indicating adsorbed oxygen on the surface of the sample.[30] After performing the UVO treatment for 15 and 30 min, a new peak of O 1s appeared at 531.0 eV, indicating that the O^{2-} peak bonded with Mo^{6+}.[30] Furthermore, the intensity of the O 1s peak located at 532.3 eV decreased on increasing the UVO treatment time. These results suggest that the MoS_2 nanosheets are converted to MoO_x by UVO treatment.

The change in the work function of MoS_2 after each treatment in the fabrication of the OPV was measured by using secondary electron emission spectroscopy, as shown in Fig. 4. The onset of the secondary electron was determined by extrapolating two solid lines from the background and straight onset in the spectra.[31]

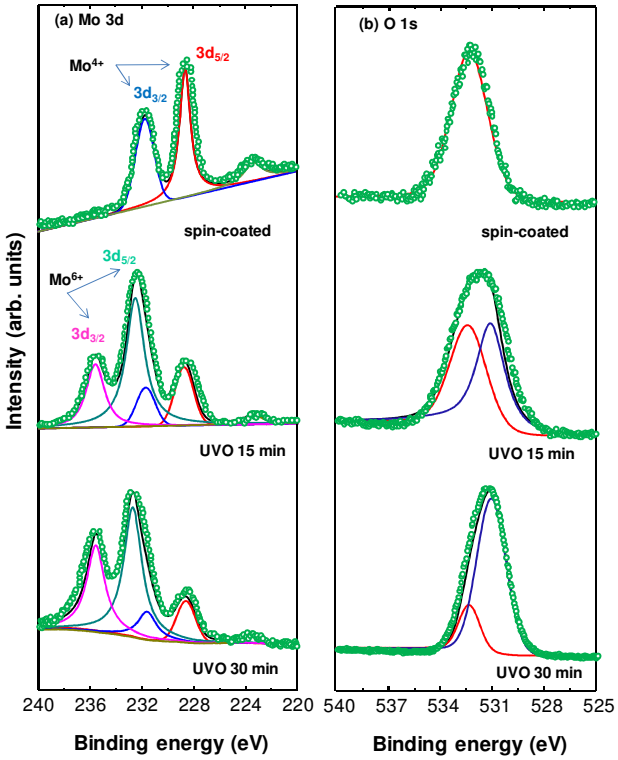

Fig. 3 SRPES spectra of (a) Mo 3d and (b) O 1s peaks according to UVO treatment time. The spectral line shape was simulated using a suitable combination of Gaussian and Lorentzian functions to separate the chemical bonding states. For all multiplets that were fit, the full-width at half-maximum values were fixed accordingly.

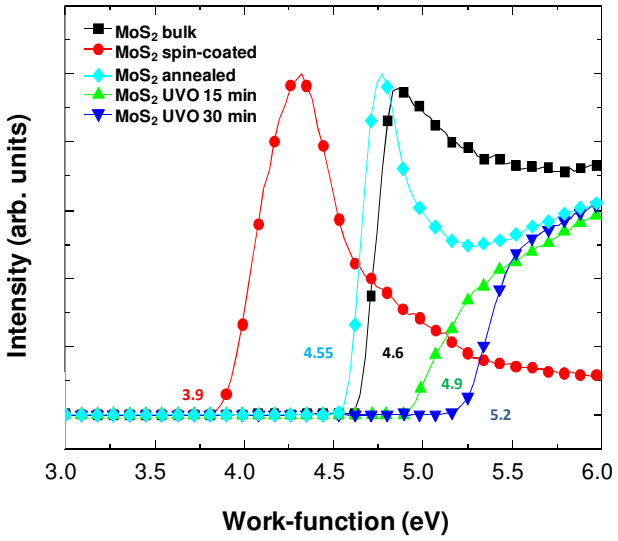

Fig.4 Change in onset of secondary electron of MoS_2 in the bulk, spin-coated, annealed states, and after UVO treatment for 15 and 30 min.

The work function of MoS_2 was measured to be 4.6 eV. The onset of the secondary electron of MoS_2 shifted by 0.7 eV to a lower work function after dipping in the DMF solvent. After the sample was annealed at 150 °C for 30 min, the work function was recovered to 4.55 eV. The work function increased to 4.9 and 5.2 eV after performing the UVO treatment of MoS_2 for 15 and 30 min, respectively. It is considered that the UVO treatment changes MoS_2 to MoO_x, leading to an increase in the work

function. This result indicates that the UVO-treated MoS_2 is adequate for use as the HEL in OPV devices.

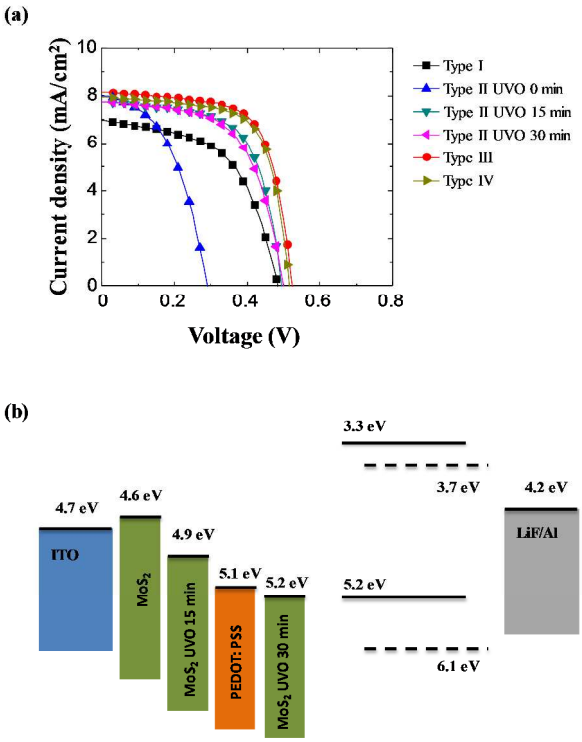

Fig. 5 (a) *J*–*V* characteristics of the devices according to the device structure and UVO irradiation time. (b) Schematic band diagram of OPV cells.

Figure 5(a) shows the *J*–*V* curves of OPV cells based on the device structure and UVO irradiation time. Same experiments were performed at least five times to confirm the effect of MoS_2. The Type-II device without UVO irradiation shows the lowest PCE of 1.08%, with J_{sc} = 8.03 mA/cm^2, V_{oc} = 0.29 V, and *FF* = 46%, which are much lower than the values of the Type-I device, which has a PCE of 1.84% with J_{sc} = 6.98 mA/cm^2, V_{oc} = 0.48 V, and *FF* = 55%. After performing the UVO treatment of the MoS_2 layer for 15 min, the PCE of the Type-II device improved to 2.44%, with J_{sc} = 7.74 mA/cm^2, V_{oc} = 0.50 V, and *FF* = 63%. These phenomena can be explained by the change in the work function of MoS_2 upon UVO irradiation. The work function of the spin-coated MoS_2 nanosheets was 3.9 eV, as shown in Fig. 4, which is not suitable for the HEL in OPV cells. Although the work function of the MoS_2 layer increased to 4.6 eV upon annealing at 150 °C, it was still not sufficient for transferring holes to the electrode. After performing the UVO treatment for 15 and 30 min, the work function of MoS_2 reached 4.9 and 5.2 eV, respectively, decreasing the hole-extraction barrier and improving the device performances, as shown in Fig. 5(b). The energy levels of ITO, PEDOT:PSS, P3HT:PCBM, and LiF/Al were obtained from other literature.[32, 33] It is shown that upon performing the UVO treatment for 30 min, the Type-II device properties are degraded in comparison with those after performing the UVO treatment for 15 min. It is considered that UVO treatment for a period longer than the optimized duration damages the MoS_2 surface, inducing the breakdown of the MoS_2 network. These data indicate that UVO has a strong effect on devices with MoS_2 nanosheets. Although the properties of the Type-II device that has undergone the UVO treatment for 15 min improved, they were still lower than those of the Type-III device, with PCE = 2.87%, J_{sc} = 8.14 mA/cm^2, V_{oc} = 0.52 V, and *FF* = 68%. In the case of the Type-IV device with both PEDOT:PSS and UVO-treated MoS_2 nanosheets, the values of PCE, J_{sc}, V_{oc}, and *FF* were 2.81%, 7.97 mA/cm^2, 0.52 V, and 68%, respectively. The properties of the Type-III and Type-IV devices are similar, and superior to those of Type-I and Type-II devices. A summary of the device properties is given in Table I. These results indicate that the UVO-treated MoS_2 nanosheets could play the role of the PEDOT:PSS layer; however, more treatments on MoS_2 are needed to improve the device properties.

Table 1 Summary of OPV properties according to device structure and UVO irradiation time.

	J_{sc} (mA/cm^2)	V_{oc} (V)	*FF* (%)	PCE (%)
Type I	6.98	0.48	55	1.84
Type II without UVO	8.03	0.29	46	1.08
Type II with UVO 15 min	7.74	0.50	63	2.44
Type II with UVO 30 min	7.76	0.50	59	2.31
Type III	8.14	0.52	67	2.87
Type IV	7.97	0.52	68	2.81

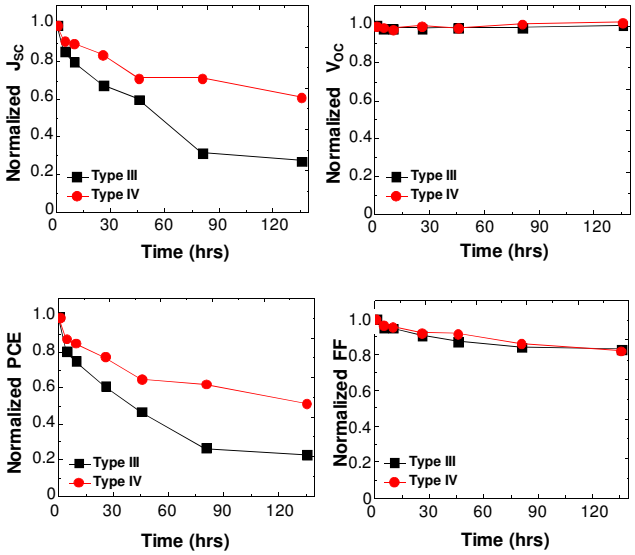

Fig. 6 Stability of Type-III and Type-IV devices measured under air without encapsulation: (a) normalized J_{sc}, (b) normalized V_{oc}, (c) normalized PCE, and (d) normalized *FF* according to the time kept in air. Each property was normalized against its initial value.

The stability of the Type-III and Type-IV OPVs was investigated under an air atmosphere without encapsulation. Figure 6 shows the (a) normalized J_{sc}, (b) normalized V_{oc}, (c) normalized PCE, and (d) normalized *FF* on the basis of the time the OPVs are kept in air. Each property was normalized against its initial value. Regarding V_{oc} and *FF*, no significant difference was found between Type III and Type IV, although the V_{oc} value was

maintained and the *FF* value decreased to 0.85 as the time was extended to approximately 120 h. The values of J_{sc} and PCE decreased to 0.6 for Type IV and 0.2 for Type III after keeping the devices for 120 h in air, indicating that a longer lifetime was achieved for devices using MoS_2/PEDOT:PSS layers than for those employing only the PEDOT:PSS layer. It seems that most of the degradation difference between the two types of OPVs was owing to the decrease in J_{sc}. Previous studies have shown that the acidity and hygroscopicity of PEDOT:PSS causes damage to both the PEDOT:PSS/ITO surface and itself.[8, 10] Thus, it is considered that the difference in device degradation between Type III and Type IV is owing to the HEL and interface degradation. These results indicate that sandwiching the MoS_2 layer between PEDOT:PSS and ITO could extend the stability of OPV cells by protecting the ITO surface from the hygroscopic nature of PEDOT:PSS.

4 Conclusion

MoS_2 was exfoliated by using the sonication method and applied to OPVs as the HEL. The increase in the wavenumber and reduction of the energy difference in the E^1_{2g} and A^1_g modes of the Raman spectra and the appearance of a UV absorption peak suggested that the layer thickness of MoS_2 decreased upon sonication. Furthermore, the AFM images confirmed that the thickness and lateral size of the MoS_2 nanosheets exfoliated by sonication were approximately 1 and 100–300 nm, respectively. After the UVO treatment on MoS_2, Mo^{6+} and O^{2-} bonded with the Mo^{6+} peaks appearing in the SRPES results, and the work function increased from 4.6 to 4.9–5.2 eV. The use of UVO-treated MoS_2 nanosheets as the HEL in OPV cells increased their PCE value to 2.44% (from 1.84% for the OPV cell without the HEL). It is considered that the work-function modulation of MoS_2 upon UVO treatment enhances its hole-extraction property. The PCE value of the OPV with MoS_2/PEDOT:PSS was 2.81%, which is comparable to that of the OPV with only the PEDOT:PSS layer. However, the use of the MoS_2/PEDOT:PSS layer extended the air stability of the OPV cells by protecting the ITO surface from the hygroscopic nature of PEDOT:PSS. Therefore, it is considered that damage caused by the acidic nature of PEDOT:PSS could be prevented by sandwiching MoS_2 between the ITO/glass substrate and PEDOT:PSS without any degradation of the device performance.

Acknowledgements

This research was supported in part by the Mid-career Research Program (2011-0028752) through the National Research Foundation of Korea (NRF) funded by the Ministry of Education Science and Technology, and in part by the Center for Green Airport Pavement Technology (CGAPT) of Chung-Ang University.

Notes and references

[a]*School of Chemical Engineering and Materials Science, Chung-Ang University 221, Heukseok-dong, Dongjak-gu, Seoul 156-756, Republic of Korea.*

[b]*Department of Materials Science and Engineering, Seoul National University, Seoul 151-744, Republic of Korea*

**E-mail: sooyoungkim@cau.ac.kr, Tel.: 82-2-820-5875, Fax: 82-2-824-3495.*

1. F. C. Krebs, *Sol. Energy Mater. Sol. Cells*, 2009, **93**, 465-475.
2. F. C. Krebs, S. A. Gevorgyan and J. Alstrup, *J. Mater. Chem.*, 2009, **19**, 5442-5451.
3. J. Alstrup, M. Jørgensen, A. J. Medford and F. C. Krebs, *ACS Appl. Mater. Interfaces*, 2010, **2**, 2819-2827.
4. Y. Park, D. W. Suh, K. S. Choi, J. S. Yoo, J. Ham, J.-L. Lee and S. Y. Kim, *Org. Electron.*, 2013, **14**, 1021-1026.
5. Y. Park, K. S. Choi, H. Yang and S. Y. Kim, *Thin Solid Films*, 2013, **537**, 217-220.
6. Y. Liang, Z. Xu, J. Xia, S. T. Tsai, Y. Wu, G. Li, C. Ray and L. Yu, *Adv. Mater.*, 2010, **22**, E135-138.
7. X. Zhan, Z. a. Tan, B. Domercq, Z. An, X. Zhang, S. Barlow, Y. Li, D. Zhu, B. Kippelen and S. R. Marder, *J. Am. Chem. Soc.*, 2007, **129**, 7246-7247.
8. M. P. de Jong, L. J. van IJzendoorn and M. J. A. de Voigt, *Appl. Phys. Lett.*, 2000, **77**, 2255-2257.
9. K. Kawano, R. Pacios, D. Poplavskyy, J. Nelson, D. D. C. Bradley and J. R. Durrant, *Sol. Energy Mater. Sol. Cells*, 2006, **90**, 3520-3530.
10. M. Jørgensen, K. Norrman and F. C. Krebs, *Sol. Energy Mater. Sol. Cells*, 2008, **92**, 686-714.
11. W. J. Dong, G. H. Jung and J.-L. Lee, *Sol. Energy Mater. Sol. Cells*, 2013, **116**, 94-101.
12. H. Pan, L. Zuo, W. Fu, C. Fan, B. Andreasen, X. Jiang, K. Norrman, F. C. Krebs and H. Chen, *Org. Electron.*, 2013, **14**, 797-803.
13. V. Shrotriya, G. Li, Y. Yao, C.-W. Chu and Y. Yang, *Appl. Phys. Lett.*, 2006, **88**, 073508.
14. J.-S. Huang, C.-Y. Chou, M.-Y. Liu, K.-H. Tsai, W.-H. Lin and C.-F. Lin, *Org. Electron.*, 2009, **10**, 1060-1065.
15. J. R. Manders, S.-W. Tsang, M. J. Hartel, T.-H. Lai, S. Chen, C. M. Amb, J. R. Reynolds and F. So, *Adv. Funct. Mater.*, 2013, **23**, 2993-3001.
16. H. Choi, B. Kim, M. J. Ko, D.-K. Lee, H. Kim, S. H. Kim and K. Kim, *Org. Electron.*, 2012, **13**, 959-968.
17. S. B. Lee, J. Ho Beak, B. h. Kang, K.-Y. Dong, Y.-Y. Yu, Y. Doo Lee and B.-K. Ju, *Sol. Energy Mater. Sol. Cells*, 2013, **117**, 203-208.
18. M. Bernardi, M. Palummo and J. C. Grossman, *Nano Lett.*, 2013, **13**, 3664-3670.
19. Y. Yu, C. Li, Y. Liu, L. Su, Y. Zhang and L. Cao, *Sci. Rep.*, 2013, **3**, 1866.
20. O. El Beqqali, I. Zorkani, F. Rogemond, H. Chermette, R. B. Chaabane, M. Gamoudi and G. Guillaud, *Synth. Met.*, 1997, **90**, 165-172.
21. J.-M. Yun, Y.-J. Noh, J.-S. Yeo, Y.-J. Go, S.-I. Na, H.-G. Jeong, J. Kim, S. Lee, S.-S. Kim, H. Y. Koo, T.-W. Kim and D.-Y. Kim, *J. Mater. Chem. C*, 2013, **1**, 3777.
22. X. Li, W. Zhang, Y. Wu, C. Min and J. Fang, *ACS Appl. Mater. Interfaces*, 2013, **5**, 8823-8827.
23. X. Gu, W. Cui, H. Li, Z. Wu, Z. Zeng, S.-T. Lee, H. Zhang and B. Sun, *Adv. Energy Mater.*, 2013, **3**, 1262-1268.
24. S. Kato, R. Ishikawa, Y. Kubo, H. Shirai and K. Ueno, *Jpn. J. Appl. Phys.*, 2011, **50**, 071604.
25. A. Molina-Sánchez and L. Wirtz, *Phys. Rev. B*, 2011, **84**, 155413.
26. L. Chen, P. Wang, F. Li, S. Yu and Y. Chen, *Solar Energy Materials and Solar Cells*, 2012, **102**, 66-70.
27. Y. R. Zhang, Y. Z. Xu, Y. Xia, W. Huang, F. A. Liu, Y. C. Yang and Z. L. Li, *J. Colloid Interface Sci.*, 2011, **359**, 536-541.
28. V. Stengl and J. Henych, *Nanoscale*, 2013, **5**, 3387-3394.
29. R. S. Sundaram, M. Engel, A. Lombardo, R. Krupke, A. C. Ferrari, P. Avouris and M. Steiner, *Nano Lett.*, 2013, **13**, 1416-1421.
30. I. Shakir, M. Shahid and D. J. Kang, *Chem. Commun.*, 2010, **46**, 4324-4326.
31. K. S. Choi, Y. Park and S. Y. Kim, *J. Nanosci. Nanotechnol.*, 2013, **13**, 3282-3287.
32. K. C. Kwon, W. J. Dong, G. H. Jung, J. Ham, J.-L. Lee and S. Y. Kim, *Sol. Energy Mater. Sol. Cells*, 2013, **109**, 148-154.
33. Y. Kim, A. M. Ballantyne, J. Nelson and D. D. C. Bradley, *Organic Electronics*, 2009, **10**, 205-209.